

Mixing enhancement in a multi-stream injection nozzle

Peter Vorobieff · C. Randall Truman · Adam M. Ragheb · Gregory S. Elliott ·
Julia K. Laystrom-Woodard · Darren M. King · David L. Carroll ·
Wayne C. Solomon

Received: 30 December 2009 / Revised: 12 February 2011 / Accepted: 25 March 2011
© Springer-Verlag 2011

Abstract We present quantitative analysis of image sequences of multi-stream injection nozzle flows with several different injection geometries in an experiment simulating mixing in a chemical oxygen-iodine laser. To visualize mixing, image sequences were acquired with planar laser-induced fluorescence (PLIF) in iodine that was injected into the main flow. The injection nozzle consisted of a slot, ejector, and injector block, with rows of ejector and injector holes along the slot length. The ejector flow exits in an underexpanded state so that upon expanding it

forces the slot and injector flows together to enhance mixing. For this study, the diameter and geometry of ejector holes were varied to assess their effect on mixing. Two configurations of ejector holes were used, each with two different diameters for a total of four cases with data collected at downstream stations. We carry out a quantitative mixing analysis for these configurations, using two methods to quantify the mixing. The first method considers the statistics of the PLIF image intensity histograms, which are bimodal for poorly-mixed flows and have a single peak in well-mixed flows. The second method quantifies the properties of the mixing interface. Our analysis shows that two injection schemes significantly enhance mixing by stretching the mixing interface.

P. Vorobieff (✉) · C. R. Truman
Department of Mechanical Engineering, The University of New Mexico, MSC01 1150, Albuquerque, NM 87131, USA
e-mail: kalthoth@unm.edu

C. R. Truman
e-mail: truman@unm.edu

A. M. Ragheb · G. S. Elliott
Department of Aerospace Engineering, University of Illinois at Urbana-Champaign, 306 Talbot Lab, 104 S. Wright St, Urbana, IL 61801, USA
e-mail: adam.ragheb@gmail.com

G. S. Elliott
e-mail: elliottg@illinois.edu

J. K. Laystrom-Woodard · D. M. King ·
D. L. Carroll · W. C. Solomon
CU Aerospace L.L.C., 301 N. Neil St., Suite 400,
Champaign, IL 61820, USA
e-mail: laystrom@cuaerospace.com

D. M. King
e-mail: king@cuaerospace.com

D. L. Carroll
e-mail: carroll@cuaerospace.com

W. C. Solomon
e-mail: solomon@cuaerospace.com

1 Introduction

The chemical oxygen iodine laser (COIL) was originally developed at the Air Force Weapons Laboratory (McDermott et al. 1978). Like all chemical lasers, COIL is powered by a chemical reaction and produces coherent light at a wavelength of 1.315 μm . The chemistry and physics of COIL lasing are generally well understood and described in detail by Avizonis and Neumann (1986), Truesdell et al. (1992), Avizonis and Truesdell (1994). Mixing is essential for driving any chemical laser as the formation rate of the excited-state species that sheds energy by lasing is limited by the mixing rate (Broadwell 1974). In a typical COIL design, the gases mix in a supersonic nozzle, with the primary flow carrying excited oxygen and a diluent (usually helium), and iodine, also with a helium diluent, forming the injected flow. Supersonic nozzles are used to maximize the temperature drop downstream of the throat of the nozzle (and thus move the state of the flow farther away

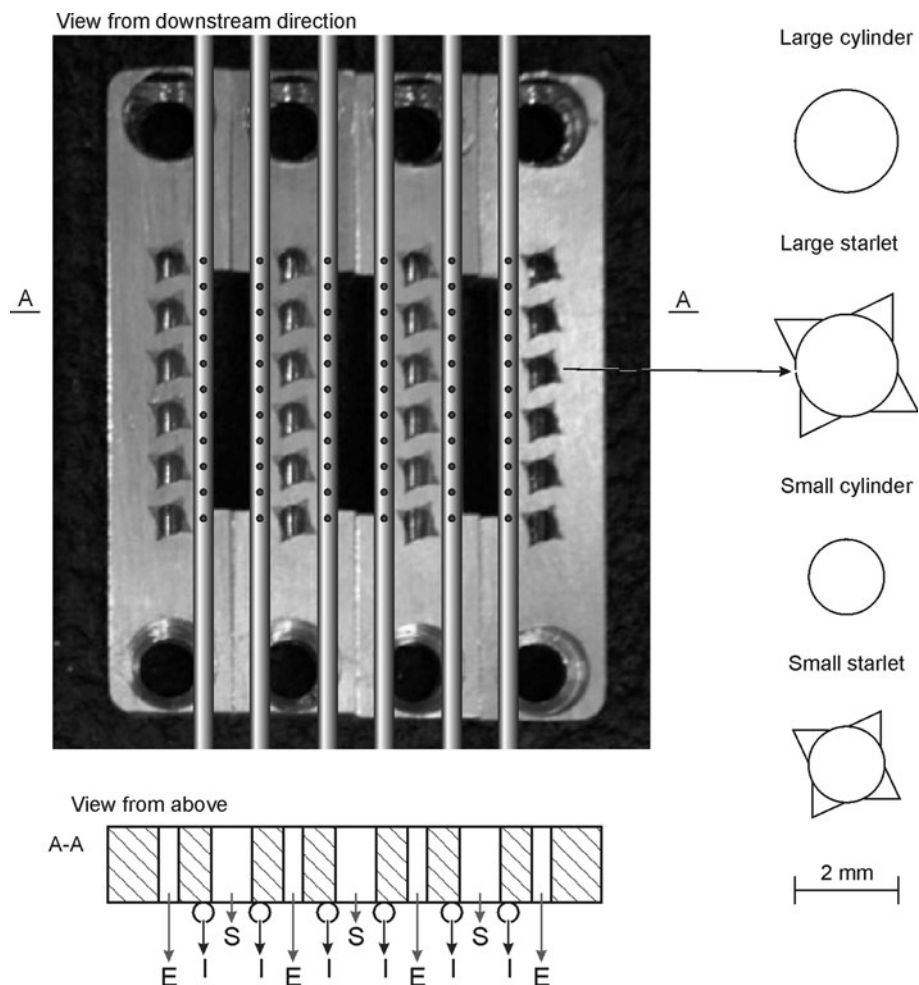
from thermodynamic equilibrium, which facilitates lasing) and to increase the flow per unit nozzle throat area. Historically, the iodine and its diluent have been injected into the subsonic region of the nozzle upstream of the throat. Injecting the iodine in the subsonic region promotes mixing between the injected iodine and the primary oxygen flows, whereas diffusive mixing is difficult in the supersonic region because of compressibility effects. However, highly efficient COIL lasers with supersonic mixing of iodine and oxygen have been developed recently (Rybalkin et al. 2003). For any injection scheme, a well-mixed medium results in more efficient lasing because the energy can be extracted more rapidly, thereby reducing kinetic quenching losses, and also produces a more uniform laser beam profile.

Different methods have been used to control (and enhance) mixing in chemical lasers, including trip and ramp nozzles (Driscoll 1986), and recently trip jets (Noren et al. 2010). A promising mixing-enhancing compact COIL configuration was developed by Nikolaev and Zagidullin (2000), who used an underexpanded driver gas to aid in the mixing of an ideally expanded flow and an underexpanded

one. This design uses three flows—slot, ejector, and injector and is thus referred to as the SEI design (Fig. 1, left). As described by Nikolaev et al. (2002), this configuration was developed to enhance the mixing between the flows emanating from the injectors and the slots at higher total pressures. The ejector flow is at a very high pressure, exiting the ejectors at a Mach number of unity and in an underexpanded state. The slot flow, due to the large cross-sectional area of the slot and the relatively low flow rate, exits the slots at a subsonic speed and very near a properly-expanded state. The injector flow, like the ejector flow, exits the injectors in an underexpanded state, at a Mach number of or very near to, unity. Immediately downstream of the SEI block face, the high-pressure ejector flow expands and compresses the flows of both the slot and injector flows while forcing the injector flow into the slot flow. The redirection of the injector flows on both sides of the slot forms an aerodynamic throat that accelerates the slot flow to a Mach number of unity (Nikolaev et al. 2002).

Recent studies aimed at further improvement of mixing in an COIL laser with an SEI nozzle block investigated the effects of changes in the ejector nozzle geometry, using

Fig. 1 Schematic of the SEI (slot-ejector-injector) design for a COIL laser. *Left column* view of SEI block from the downstream direction (*top*) and cross-section of the block (*bottom*) with slot, ejector, and injector flows marked as *S*, *E*, and *I* respectively. In the left column, the SE (slot-ejector) plate with large starlet ejectors used in our experiments is shown. *Right column* schematic of ejector geometries. *Scale* shown refers to right column only



Schlieren and planar laser induced fluorescence (PLIF) to visualize the flow forming downstream of the SEI block (Ragheb et al. 2010a, b). These studies used two different sizes of ejectors, as well as altered ejector geometry (notched cylindrical ejectors, or “starlets”), based upon the design of Carroll and Solomon (2005, Private communication). The idea of the “Starlet” nozzle concept stems originally from experimental work of Pannu and Johannesen (1976). Pannu and Johannesen (1976) reported results from a series of experiments with sonic flow from tubes with *V*-shaped slots cut into the end of the tube. Our interest in these experiments concerns the flow field generated by the slots that create two counter-rotating vortices at each notch. Notably, these vortices generate a large outward flow velocity, thereby stretching the surface of the mixing interface. The notches essentially create a high degree of strain or fluid stretch to accelerate the molecular mixing. Smaller “starlet” ejectors appear to provide the best mixing among the geometries studied by Ragheb et al. (2010a, b). Here, we present a quantitative investigation of mixing in the same SEI laser based on ensembles of PLIF images acquired in a downstream plane normal to the mean flow direction, and quantitatively assess the efficiency of mixing associated with different ejectors.

2 Experimental arrangement and diagnostic system

The experimental setup used an SEI block inspired by Nikolaev et al. (2002) and shown in Fig. 1. Downstream of this block, a square cross-section test section/cavity ($12.7 \times 12.7 \times 40.6$ cm) was mounted. The cavity was fitted with four large view windows for flow visualization (Fig. 2). The minimum pressure that could be achieved in the cavity with no flow present was ~ 0.5 Torr, with the

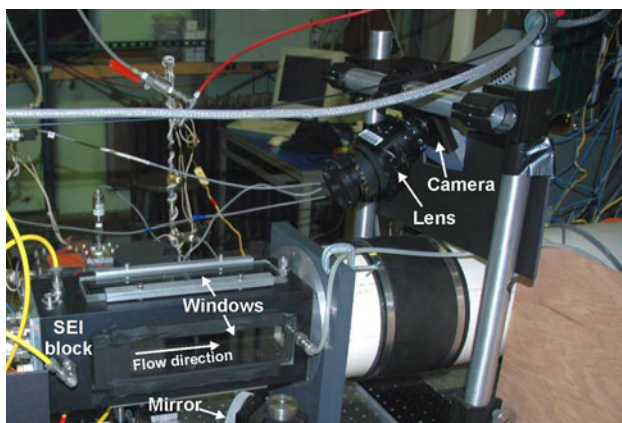


Fig. 2 View of the experimental arrangement. The SEI block is on the left, the cavity with view windows is on its right side. Individual components are labeled in the picture

vacuum system driven by a Kinney KT-850 single-stage rotary vacuum pump powered by a 50 HP electric motor, and by an MD-90 Roots blower, powered by a 5 HP motor, installed in series with the pump.

The system was equipped with a United Sensor Corporation (USC) PDA-12-F-11.84-KL pitot-static probe attached to two MKS Baratron 722 high-accuracy pressure transducers and mounted on a precision translation stage. Measurements of the flows entering the cavity from the SEI block were taken with two Micro Motion Elite CMF025H and one CMF010H Mass Flow Sensors. One sensor each was installed in line with the slot, ejector, and injector flows, and preexisting calibrations were used for each different gas.

The primary diagnostic used in this work was PLIF, with fluorescence in iodine induced by 532-nm coherent light from a Quantel Brilliant B frequency-doubled Nd:YAG laser. Laser optical energy at this wavelength was about 450 mJ per pulse. The laser pulse frequency was 10 Hz, which would preclude acquisition of time-resolved image sequences but was quite sufficient for acquiring ensembles of temporally uncorrelated images at a specific spatial location. A planar section of the flow (for all the data in the next section, this section was normal to the mean free-stream direction) was illuminated with a laser sheet. The laser sheet was formed by redirecting the laser beam with three dichroic mirrors and expanding it with a combination of cylindrical and plano-convex lenses. The latter lens, the final dichroic mirror (Fig. 2, bottom), and the camera used to capture the images were mounted on the same sliding optical breadboard, to facilitate image acquisition at different downstream locations without extensive refocusing or realignment, as well as to retain consistent pixel resolution during visualization of cross-flow planes at different downstream locations.

The camera is a GEN III intensified, gated CCD (charge-coupled device) Andor iStar, with a resolution of 512×512 pixels. The geometry of the test section made it impossible to aim the camera at the SEI block directly from the downstream. Thus, the camera was angled at 30° down with respect to the horizontal direction and positioned above the test section. A combination of an *f*/1.4 85-mm Nikkor lens and an *f*/2.8 Nikkor perspective correcting lens was mounted on the camera. The optics on the camera were tuned as follows. In the plane of the laser sheet, a dotcard (a calibrated target with evenly spaced dots) was positioned. Then the perspective correcting lens was manually adjusted to make all the dots on the target appear evenly spaced and in focus. Here, we consider any distortion effects on the images recorded by the camera to be negligible. The final component of the camera optics was a Kintek holographic notch filter with an optical density better than 6.0 at 532 nm. This filter removed the light

produced by the Nd:YAG laser, facilitating capture of fluorescence images, with the characteristic fluorescence wavelength at about 568 nm.

The timing of the camera was dictated by two considerations. First, the camera had to capture the iodine fluorescence. Second, the presence of the notch filter notwithstanding, it was desirable to avoid taking exposures during the laser pulse inducing fluorescence, to eliminate any possibility of capturing background laser scattering. With the characteristic laser pulse duration of about 7 ns, and the characteristic iodine fluorescence lifetime of about 1,500 ns (Sakurai et al. 1971), it was possible to satisfy both considerations by delaying the camera trigger by 60 ns with respect to the trigger for the laser.

Four ejector geometries shown in Fig. 1 (right column) were imaged at ejector flow rates of 200, 686, and 1,000 mmol/s, a slot flowrate of 32.1 mmol/s, and an iodine-seeded injector flow rate of 6.9 mmol/s prior to the iodine being introduced into the flow. For the 686 mmol/s data analyzed here, the flow velocity of the N₂ ejector stream (sonic) was about 383 m/s, the velocity of the N₂/I₂ injectors (sonic) is estimated to be 318 m/s, and the velocity of the slot flow (assuming aerodynamic choking near the exit of the slot) is estimated to be 104 m/s. The flows are pure N₂, except for the injector flow, where the iodine injector tubes have approximately 0.03 mmol/s (30 micromoles/s) of I₂ seeded into the flow.

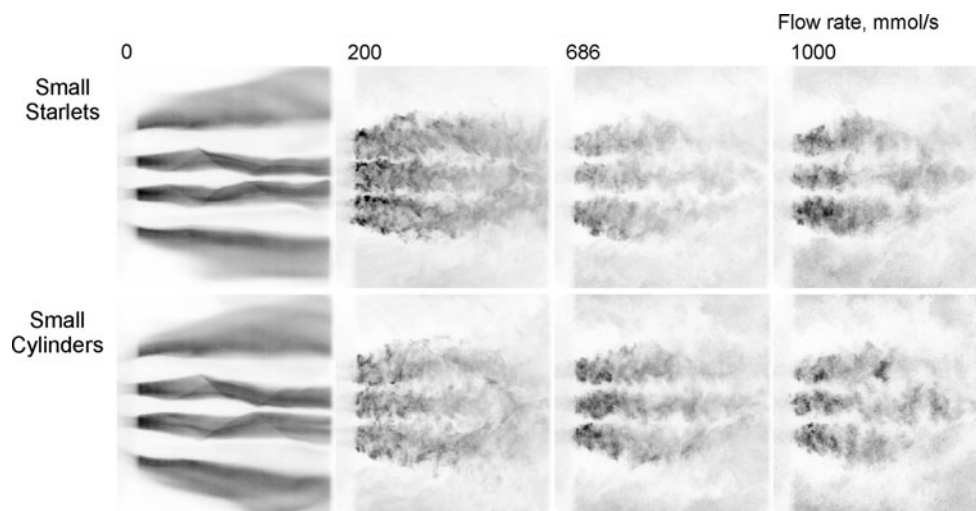
Fluorescence and background images were recorded in stacks of 100, and the background was subtracted prior to the analysis described in the next section. The data presented in the next section corresponds to the case when the flow rate from the ejectors was at 686 mmol/s, with other cases discussed and compared elsewhere (Ragheb et al. 2010b). For this ejector flow rate, the pressure in the cavity was 17.3 Torr with large ejectors (cylinders or starlets) and 17.6 Torr with small ejectors.

3 Results of flow visualization

Let us begin with a summary of the flow visualization study performed for different flow rates. The ejector flow rate can have significant impact upon mixing and consequently laser performance. PLIF imaging from above the test section in a horizontal plane parallel to the downstream direction (Ragheb et al. 2010b) is shown in Fig. 3 for the small cylinders and starlets as a function of the ejector flow rate (the corresponding images for the large cylinders and starlets are qualitatively similar and are not shown for brevity). The pair of images in the left column is for the zero ejector flow case. The unseeded (brighter) regions between iodine fluorescent jets represent the three slot flows. A close inspection shows that each of the central two jets actually consists of a pair of iodine jets that correspond to a pair of iodine injector tubes (Fig. 1). In the zero ejector flow case, the slot flow forces each inner pair of iodine injectors to coalesce.

Addition of the ejector flow results in a dramatic change in the character of mixing. The result is a great deal of structure and apparently much enhanced mixing (Fig. 3). From the morphologies of the horizontal PLIF images, it is difficult to distinguish the subtle differences in mixing between the cylindrical and starletted ejectors, thus necessitating the study of vertical PLIF images discussed later in this work. However, close inspection of Fig. 3 reveals interesting differences as a function of ejector flow rate. First, let us point out that when the ejector flow is added, the ejectors now force the flow from the iodine injector tubes to coalesce across the slot flows, thereby resulting in two unseeded regions between fluorescing regions (rather than three unseeded regions as in the zero ejector flow case). As the ejector flow is increased, the unseeded regions also increase in size due to:

Fig. 3 PLIF imaging in the horizontal plane for different ejector flow rates (after Ragheb et al. 2010b). The flow direction is from *left to right*, representative instantaneous images are shown. The palette is inverted, with darker tone corresponding to higher concentrations of iodine, and light background representing iodine-free (unseeded) flow



1. More core ejector flow that is not being mixed with iodine, and
2. Higher pressure in the ejector exit region that forces (pushes) the iodine streams more rapidly into the slot flow regions, thereby increasing the mixing rate near the face of the SEI block.

The effect of ejector flow rate upon COIL laser performance was recently explored in some depth by King et al. (2011) for an SEI block configuration similar to that shown in Fig. 1. It was found that the optimal ejector flow rate was dependent upon the position of the optical axis of the laser mirrors. When the optical axis was located 6.40 cm downstream from the ejector plane, laser output power was highest when the ejector flow rate was in the 200–300 mmol/s range. However, when the optical axis was only 3.86 cm downstream from the ejector plane, the ejector flow rate had to be approximately doubled to 500–600 mmol/s to obtain fast enough mixing for good laser performance (Fig. 8, King et al. 2011). This result is consistent with the PLIF imaging shown in Fig. 3, from which we conclude that higher ejector flow rates will force more rapid mixing between the iodine injector and slot flows.

As mentioned above, while PLIF data in the streamwise direction alone provides important qualitative insight into the mixing process, quantitative analysis of images in the cross-flow direction must be conducted to draw conclusions about the respective mixing quality of the flows produced by different SEI block ejectors.

Here, we analyze PLIF data stored in the form of stacks each comprised of 100 instantaneous 16-bit grayscale PLIF images with background subtracted. Schlieren was used to image the flow in the streamwise direction (Ragheb et al. 2010a). PLIF images were acquired in the vertical plane normal to the downstream direction (Ragheb et al. 2010b). Here, we concentrate on the analysis of the latter images. Those PLIF stacks were acquired at downstream locations 12.7, 25.4, 50.8, and 101.6 mm from the slot/ejector/injector block. Figure 4 shows representative instantaneous and ensemble-averaged PLIF images corresponding to two ejector geometries (small cylinders and small starlets). The images in the 12.7-mm downstream plane show the least mixing and demonstrate the differences between the flows produced by different ejectors most clearly. In planes farther downstream, the flow from different ejectors becomes harder to distinguish, and at the 101.6-mm location it appears well-mixed (here, we must note that one of the design goals is not just to achieve good mixing somewhere downstream, but to obtain it at a downstream location close to the SEI block, thus minimizing the streamwise extent of the cavity). These observations are confirmed by quantitative analysis presented below, as

well as by PLIF imaging and analysis in the horizontal plane described elsewhere (Ragheb et al. 2010b) and above. Flow downstream of other ejectors follows similar trends. Based on the patterns we observed in the downstream evolution of the flow, most of the quantitative comparison of mixing characterizing different injection geometries was carried out for the data captured in the 12.7 mm cross-flow plane—sufficiently far downstream for differences in mixing to become apparent but not far enough for the flows to become uniformly well mixed and thus not analyzable.

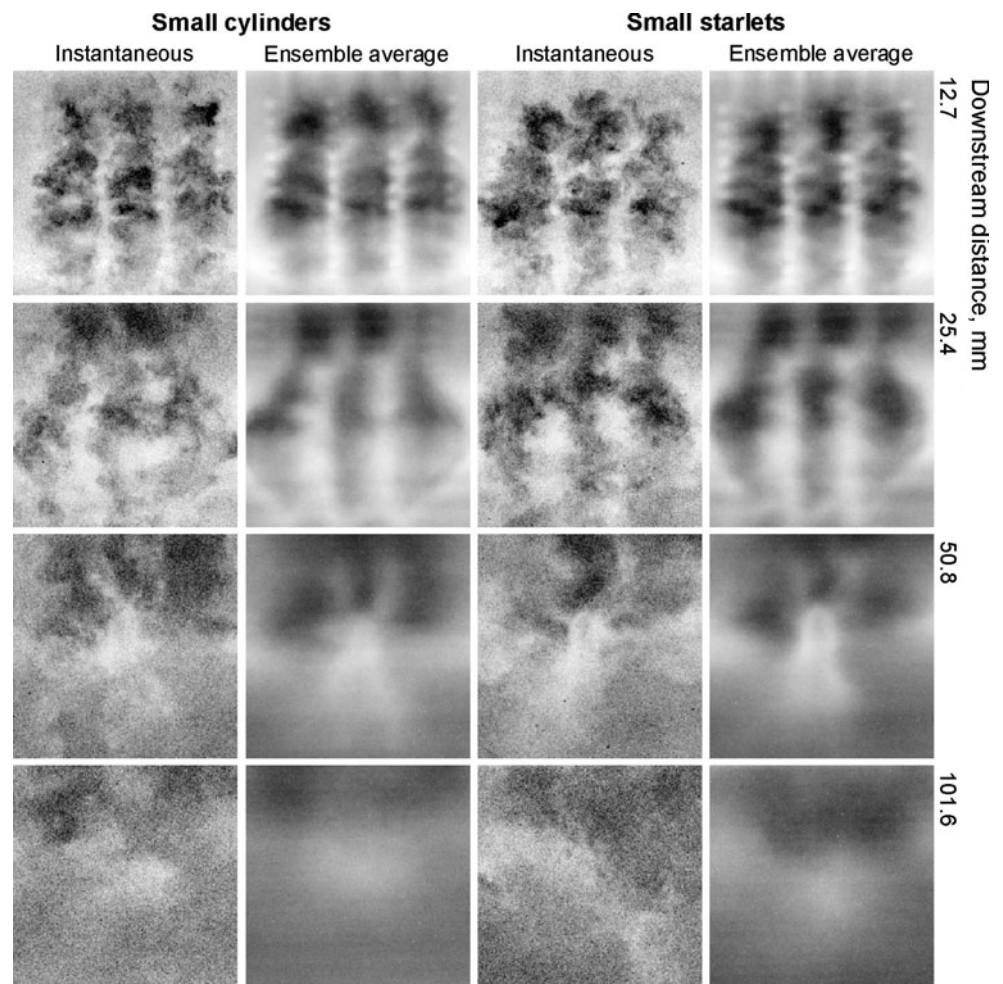
Now, let us discuss the flow features in the plane 12.7-mm downstream of the SEI block with different ejectors. The data acquisition in this plane took place under nominally identical conditions, and with the same camera settings for all the cases. Figure 5 shows representative images from each of the four stacks corresponding to the four ejector geometries. Note that these images, as well as those in the previous figures, are inverted for clarity. Thus in the following discussion, we will refer to injected material with iodine as “darker,” and to flow without the iodine as “brighter.”

In the images of all these test cases, the darkest pixels would correspond to the unmixed injected iodine flow, with the bright (background-level) pixels representing either the unmixed primary flow or the injected flow fully mixed with the primary flow, so that in the latter case, the local concentration of iodine is so low that any fluorescence is below the camera sensitivity threshold. The overall morphology of all the images is similar, with considerable irregularity and apparent mixing between the primary and injected flows. Ensemble-averaging each image stack (Fig. 6) provides some additional insight into the overall structure of the cross-sectional flow. What becomes apparent is the influence of the ejector size on the size of the large-scale structures in the cross-flow plane, with smaller ejectors (left column) leading to smaller structure size and overall better mixing. However, it would still be rather difficult to directly use even these ensemble-averaged images for mixing quality comparison, because the differences between the cases are subtle and must be addressed statistically.

4 Analysis

The cross-flow images farthest downstream from the nozzle in Fig. 4 from the previous section show the flow that appears well-mixed. However, one would be well-advised to obtain a quantitative confirmation of this notion, for example, by considering how the intensity histograms of the PLIF images change with downstream distance. Intensity histogram analysis has a well-established history

Fig. 4 PLIF visualization in cross-flow planes at four downstream distances from the slot/ejector/injector block. Each horizontal row corresponds to the downstream distance labeled to the right. Images are arranged in columns corresponding to ejector type (small cylinder or small starlet) and image type (representative instantaneous or ensemble-averaged). Images are cropped to 300×300 pixels, with 0.1-mm physical pixel resolution. The palette is inverted, with darker tone corresponding to higher concentrations of iodine, and light background representing iodine-free flow



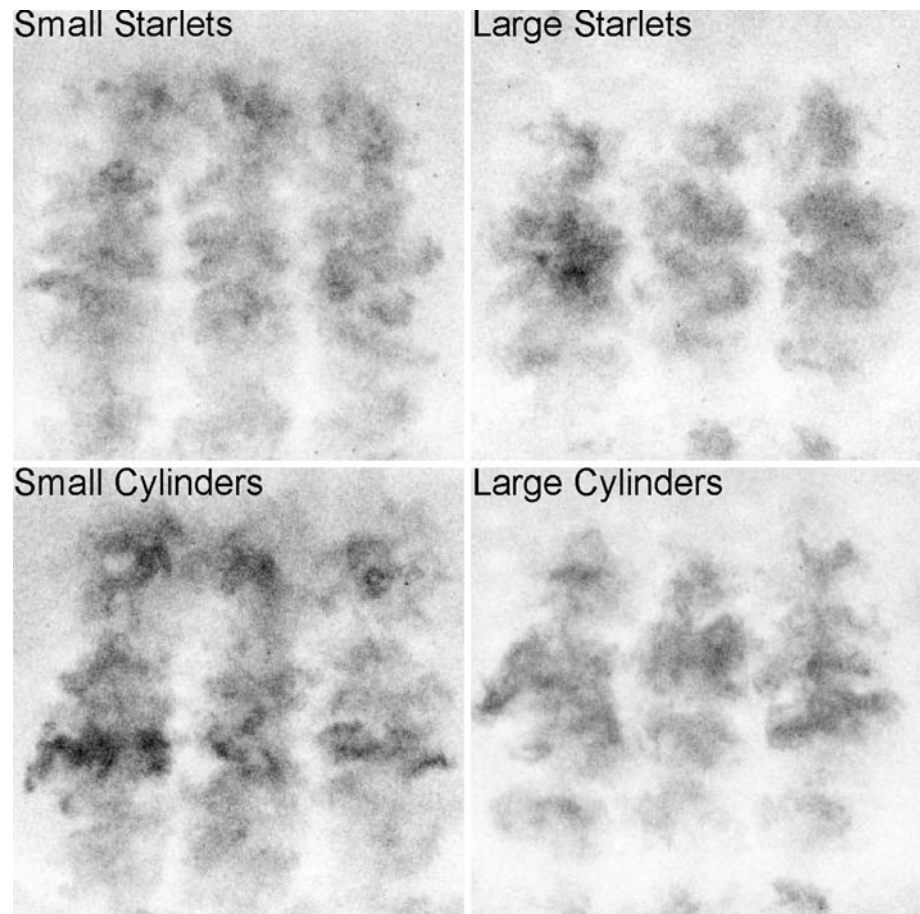
in characterization of mixing turbulent and chaotic flows (Catrakis and Dimotakis 1996; Rightley et al. 1999; Truesdell et al. 2003). Evolution of an idealized mixing flow starts with a bimodal intensity histogram, where the two peaks correspond to the two initially unmixed species, one of which is marked with a bright tracer. As the species mix, both of these peaks erode, while the gap between them is “filled” with the mixed material. Ultimately, the intensity histogram retains a single peak associated with the intensity of the diluted tracer in the well-mixed state. Here, it must be noted that the histograms discussed in the following paragraphs do not describe a flow location where that “idealized” mixing state exists, so the picture is somewhat different. Figure 7 shows a comparison of the intensity histograms obtained from the image stacks used to create Fig. 4. In these histograms, zero intensity corresponds to the background level associated with the primary (or well-mixed) flow. The greater the extent of the histogram curve to the right, the more unmixed (injected) material is present at the location.

As it becomes apparent from Fig. 7, the farthest downstream histograms for both the small cylinders and the

small starlets are rather similar and are characterized by a single intensity peak associated with well-mixed flow. There is not much difference between the histograms at that location (101.6 mm) and the preceding one (50.8 mm) either. On the other hand, histograms at the 12.7-mm location show discernible differences, with the histogram for small starlets showing lower counts of high-intensity pixels (unmixed iodine). Moreover, the plots strongly suggest that for small starlets, the flow becomes well-mixed at a downstream distance closer to the SEI block. Now, for each ejector geometry, let us compare the histograms immediately downstream of the SEI block, where differences due to different ejectors are more prominent. Figure 8 shows mixing histograms at the 12.7-mm plane corresponding to the four ejector geometries. In each case, the vertical coordinate on the histogram represents the number of the pixels at a given intensity in the corresponding image stack.

As it was mentioned above, greater extent of the histogram curve to the right indicates presence of more unmixed (injected) material at the location, thus indicating that small starlets have the best mixing, closely followed by large

Fig. 5 Instantaneous images of the cross-flow plane 12.7-mm downstream of the SEI block. Images are inverted, with darker tone corresponding to higher concentrations of iodine, and light background representing iodine-free flow. Ejector type corresponding to each image is labeled. Images are cropped to 300×300 pixels, with 0.1-mm physical pixel resolution



starlets and small cylinders, and large cylinders have poorer mixing. As the iodine cold flow rate was not directly measured in the experiments, it is not possible to directly correlate intensity with species concentration in the histogram plots. A quantitative measure that can be used to rate the mixing quality of the flow is the mixing parameter based on the first moment of the intensity histogram. Here, we use the analysis originally described by Truesdell et al. (2003), with the modifications necessitated by the fact that in our flow, the well-mixed state would have a histogram very similar to that of the primary flow with no injection, while Truesdell et al. (2003) considered the mixing of two equal volumes of fluid, resulting in a different (and easily quantifiable) well-mixed state. If $p(x)$ is the normalized intensity distribution as the function of intensity x , and I_m is the maximum intensity, the histogram centroid is

$$\bar{x} = \int_0^{I_m} xp(x)dx$$

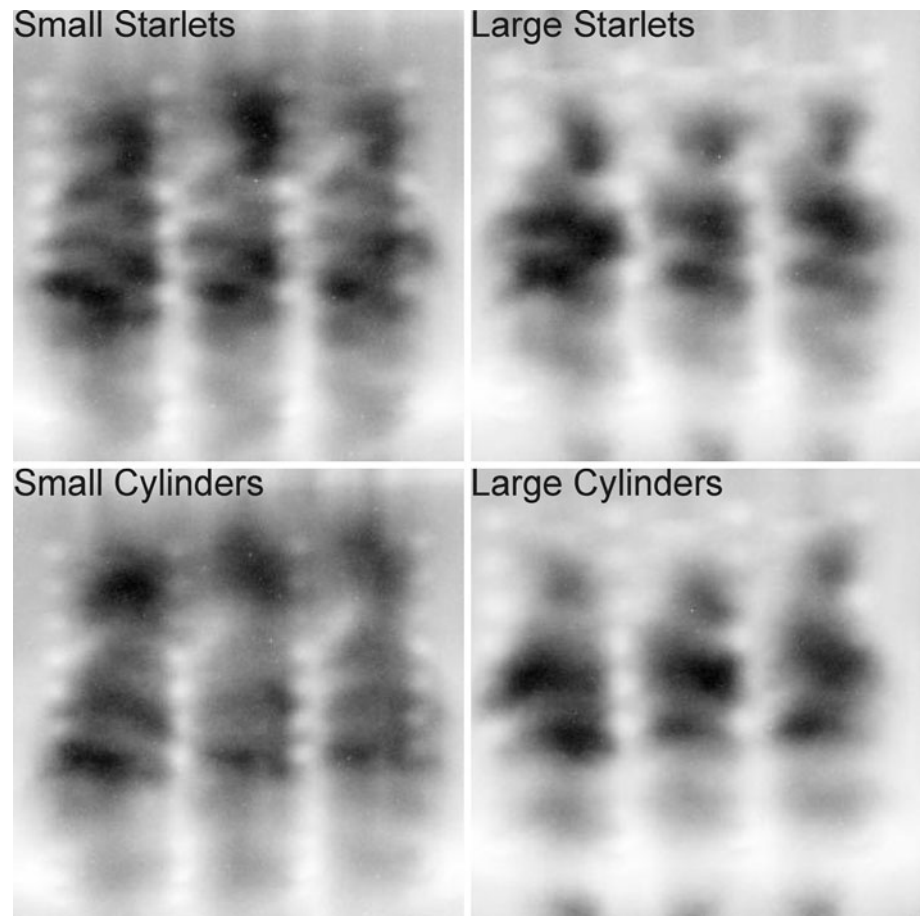
Then the mixing parameter (normalized first moment of the histogram) is

$$M_1 = \int_0^{I_m} |x - \bar{x}|p(x)dx,$$

For a single-mode, delta-function-like distribution, M_1 would approach zero. Figure 9 shows the evolution of the mixing parameter M_1 with downstream distance for small cylinders and small starlets, based on the histograms presented in Fig. 7. Far downstream, there is no discernible difference between the M_1 values. At the 12.7-mm downstream location, however, the difference between the small starlets and small cylinders is appreciable. Effectively, the starlets produce the same amount of mixing there as the cylinders do several millimeters farther downstream. This is important to know if one keeps in mind that a design goal for the chemical laser mixing nozzle is not just to achieve good mixing, but to attain it at a distance from the SEI block that simultaneously provides a high degree of iodine dissociation, minimizes chemical kinetic losses that reduce laser output power, and minimize the streamwise extent of the laser cavity.

Similarly, the inset in Fig. 9 shows the normalized first moments of the histograms from Fig. 8 corresponding to

Fig. 6 Ensemble-averaged images of the cross-flow plane 12.7-mm downstream of the SEI block. Images are inverted, with darker tone corresponding to higher concentrations of iodine, and light background representing iodine-free flow. Ejector type corresponding to each image is labeled. The image resolution is 300×300 pixels, with resolution 0.1 mm per pixel



the 12.7 mm plane, where mixing differences are more prominent, with lower values thus corresponding to higher mixing.

The values of M_1 confirm our observations of mixing quality based on the histograms of Fig. 8, with small starlets producing the best mixing and large cylinders the poorest.

An important feature of any mixing process is the mixing interface. Mixing in turbulent flows is greatly enhanced because the mixing interface (where the mixing on the microscale is always diffusive) is stretched on multiple scales by the turbulent flow field. In terms of a grayscale intensity map, the interface is a contour separating two areas where the intensity is above and below a certain threshold. If there exists an explicit relationship between the intensity and concentration of species in the flow, mixing interfaces corresponding to various species concentrations can be defined. In our case, such a relationship was not available. The mixing histograms in Fig. 8, however, present an opportunity to define the intensity level most relevant for mixing as the level where the slope of the histogram reaches its maximum as the intensity changes from high-count, low brightness primary flow to the lower-count, high brightness injected flow. This

slope can be interpreted as the spatial “mixing rate” between areas of different intensity (and concentration), with its local extremum corresponding to the intensity threshold value most relevant for mixing. This intensity threshold (about 500) turns out to be quite consistent for all the image stacks.

Using the threshold intensity values obtained thusly, we reduced the images in the data stacks to contour plots that were subsequently analyzed. Figure 10 shows representative contours for two out of four cases, illustrating relatively good and relatively poor mixing (small starlets and large cylinders). Subsequently, we analyzed the mixing interfaces for each case in terms of length and fractal dimension.

The mixing interface length (Fig. 11) was calculated for each individual image in the corresponding image stack and averaged, with the standard deviation of its value within the stack used to provide the error bars. Higher values of mixing interface length initially suggest better mixing. Far downstream, this measure would begin to degrade as most of the volume of the injected flow would become well-mixed with the primary flow, with the fluorescence becoming too faint to resolve. At the chosen downstream location, however, this degradation does not

Fig. 7 Comparison of pixel intensity histograms at different downstream distances for small cylinders (*solid line*) and small starlets (*dashed line*)

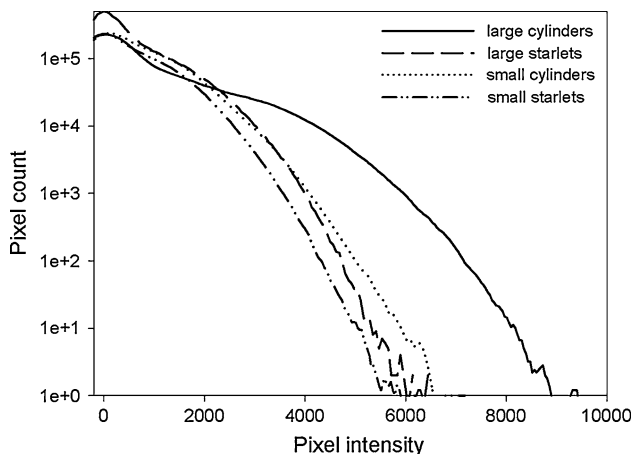
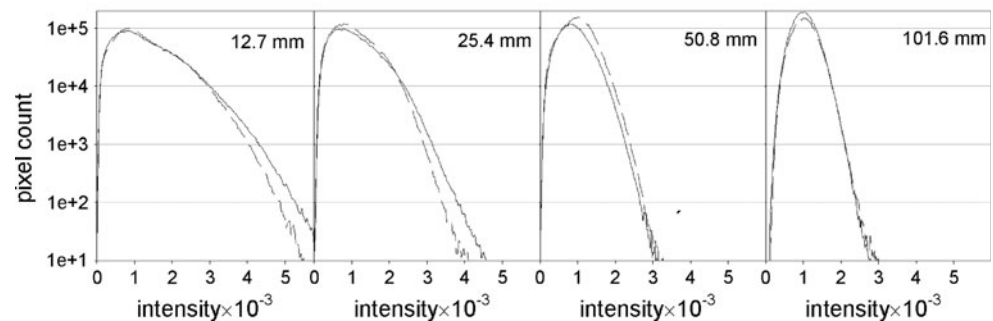
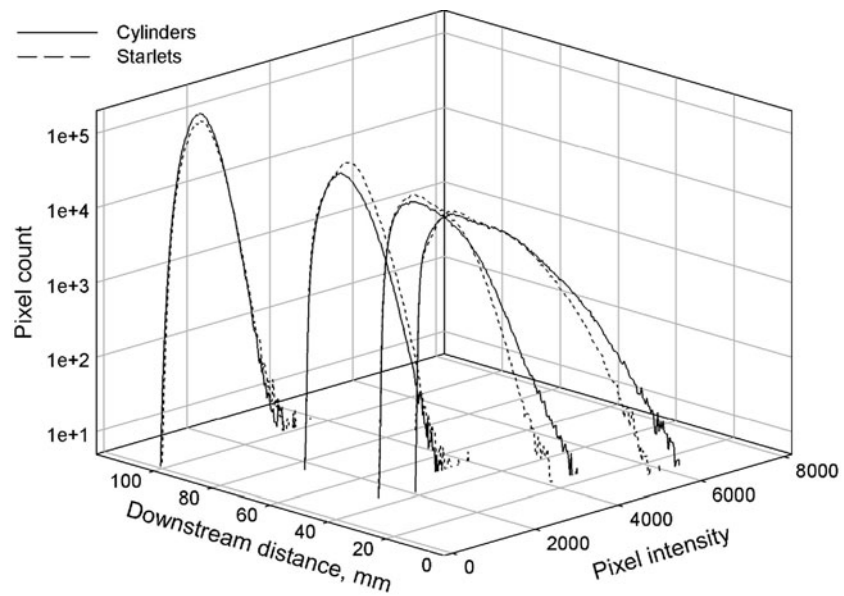


Fig. 8 Histograms of image stack pixel intensity of PLIF images in a plane normal to the freestream direction 12.7-mm downstream from the slot/ejector/injector block

yet present a problem. Based on the interface length alone, small starlets and small cylinders show the highest mixing performance, followed by large starlets and large cylinders. This ranking is largely consistent with the ranking we obtained from the histogram analysis. It is not surprising

that the interface lengths obtained from the full flow images like those shown in Fig. 5 far exceed those of the ensemble averages from Fig. 6. For comparison, the latter are shown as stars in Fig. 11; the fluctuating components of the flow have a critical influence on distorting and stretching the interface.

Another measure of mixing interface properties particularly useful for turbulent flow is the fractal dimension of the interface. In the strict mathematical sense, fractal dimension D characterizes self-similar curves filling the plane, with integer-dimension limit cases for non-fractal objects being unity for a line and two for a plane. In our case, we use the box-counting fractal dimension (Theiler 1990) mostly as a measure of the interfacial complexity. Measurements within stacks corresponding to each case were conducted using the same contours and same averaging procedures as described for interface lengths. The results are presented in Fig. 12. Large cylinders and large starlets have fractal dimension estimates ~ 1.44 – 1.47 , while small cylinder and small starlet images have fractal dimension estimates ~ 1.60 – 1.61 , indicating better mixing. Here, it is interesting to compare our results with similar measurements in turbulent and transitional mixing flows,

Fig. 9 Normalized mixing parameter M_1 as the function of downstream distance for small cylinders and small starlets. *Inset* shows M_1 values for four ejector types 12.7 mm downstream

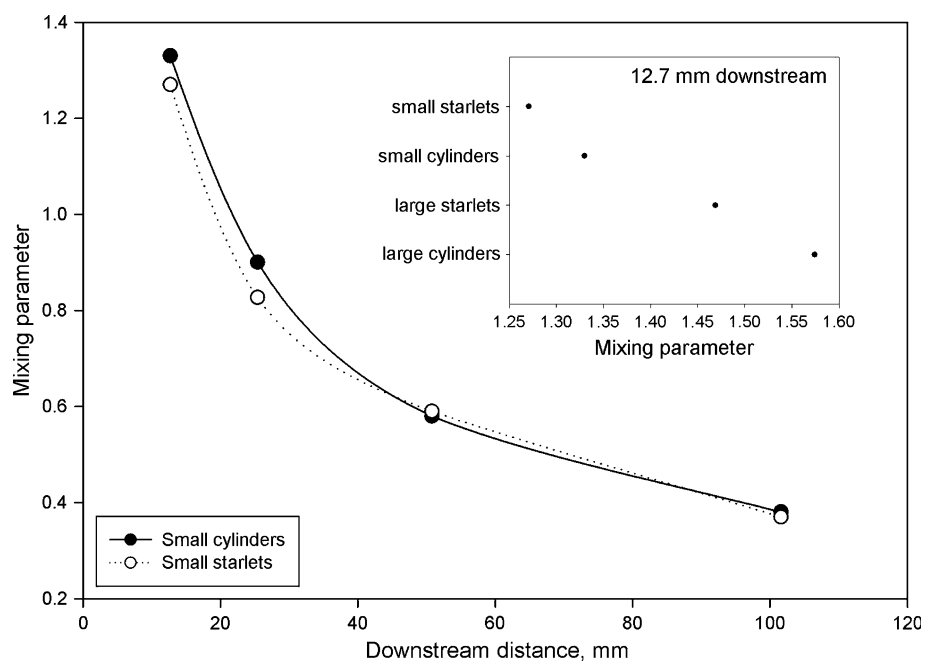
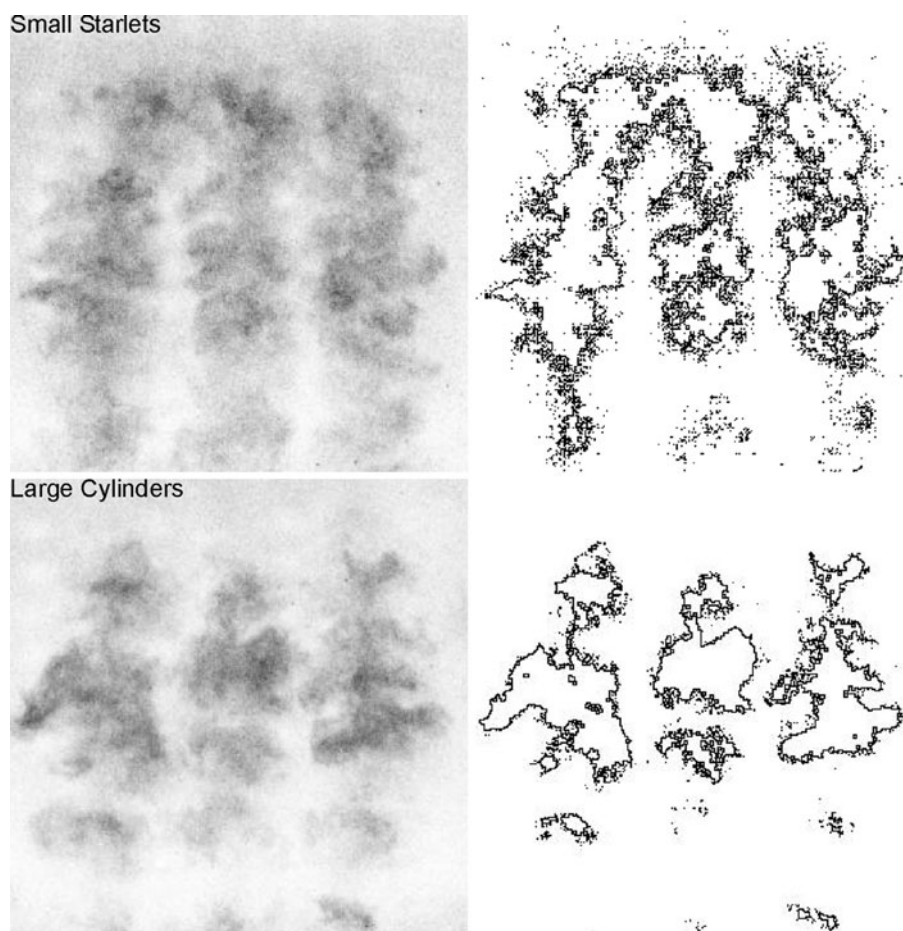


Fig. 10 Representative instantaneous flow images and corresponding mixing interfaces for cases of good mixing (*top*, small starlets) and poor mixing (*bottom*, large cylinders)



where the fractal dimension of a 2D section of the mixing interface is estimated. In turbulent or pre-turbulent flows, experimental fractal-dimension estimates on the order of

1.4 have been reported (Prasad and Sreenivasan 1990; Flohr and Olivari 1994; Vorobieff et al. 1999). Prasad and Sreenivasan (1990) also report observations of higher

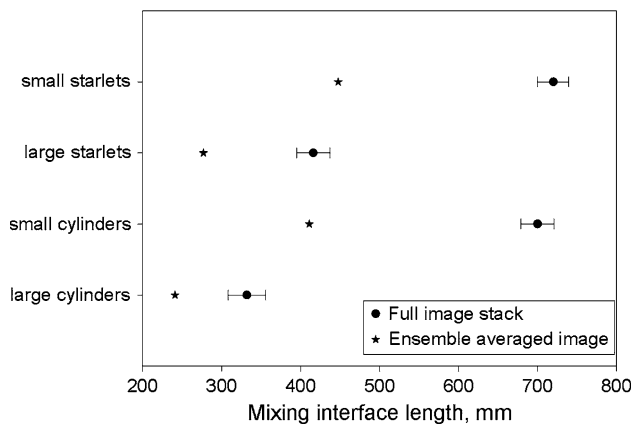


Fig. 11 Mixing interface lengths based on image stacks (*circles*) and ensemble-averaged images (*stars*)

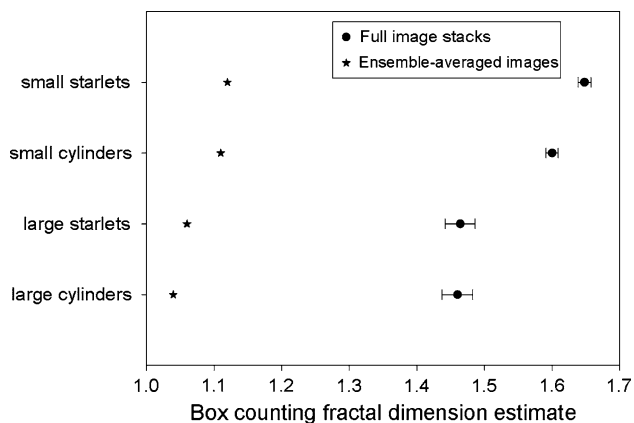


Fig. 12 Fractal dimensions of mixing interfaces

fractal dimensions (~ 1.7 for a 2D section), and explain this difference by the influence of the Schmidt number $Sc = \nu/D$, where ν is the kinematic viscosity and D is mass diffusivity. In other words, it is a measure of the relative importance of momentum and mass diffusivities. Theoretical considerations for the case when mass and momentum diffusion are equally important ($Sc \sim 1$) yield a fractal dimension $D = 1.36$ for a mixing interface in fully developed turbulent flow (Prasad and Sreenivasan 1990). On the other hand, when Prasad and Sreenivasan (1990) consider a similar theoretical argument for large Schmidt numbers, they find that in the limit case of $Sc \rightarrow \infty$, the mixing interface convolutions should be space-filling ($D \rightarrow 2$), explaining the higher fractal dimensions they observe. Let us note that while an accurate determination of the relevant Schmidt number for our system is not easy because of the fluctuations in composition, temperature, and pressure, an estimate exceeding unity may be plausible.

Once again, here for comparison, we show the fractal dimension estimates of the “mixing interfaces” of the

ensemble-averaged images from Fig. 6, which are close to trivial for all the ejector geometries.

5 Conclusions

Our analysis reveals that injection geometry strongly affects mixing, with the following trends discernible. Using smaller size ejectors (small cylinders vs. large cylinders, small starlets vs. large starlets) results in better mixing. Adding starlets to a given ejector geometry results in better mixing. Fractal dimensions of the mixing interfaces are consistent with those for fully developed turbulent flow, suggesting that further mixing enhancement by changing the ejector geometry alone might be hard to attain. Overall, small starlets produce the best mixing, closely followed by small cylinders. Large cylinders produce poorer mixing.

The authors note that this study of mixing via PLIF imaging led to a down selection of the ejector nozzle choices for COIL laser performance testing performed by King et al. (2011). The resulting outcoupled laser power from the small starlets was 20–30% higher than that from the cylindrical ejectors; this confirms our conclusions herein based upon PLIF data that the starlets provide enhanced mixing in these slot-ejector-injector block configurations.

Acknowledgments This research was funded by the US Missile Defense Agency (MDA) through a contract with the U.S. Army Space and Missile Defense Command on a Phase II SBIR program with CU Aerospace L.L.C.

References

- Avizonis P, Neumann D (1986) The chemical oxygen-iodine laser. *J Def Res* 511–524
- Avizonis P, Truesdell K (1994) Historical perspectives of the chemical oxygen-iodine laser (COIL). In: Proceedings of the 25th AIAA plasmadynamics and lasers conference, AIAA Paper 94-2416
- Broadwell J (1974) Effect of mixing rate on HF chemical laser performance. *Appl Opt* 13(4):962–967
- Catrakis H, Dimotakis P (1996) Mixing in turbulent jets: scalar measures and isosurface geometry. *J Fluid Mech* 317:369–406
- Driscoll R (1986) Mixing enhancement in chemical lasers, part I: experiments. *AIAA J* 24(7):1120–1126
- Flohr P, Olivari D (1994) Fractal and multifractal characteristics of a scalar dispersed in a turbulent jet. *Phys D Nonlinear Phenom* 76:278–290
- King D, Carroll D, Field T, Laystrom-Woodard J, Driscoll R, Sentman L, Ragheb A, Elliott G, Solomon W (2011) Performance of a multi-stream injection COIL with starlet ejectors. *AIAA J* (in press)
- McDermott WE, Pchelkin NR, Benard DJ, Bousek RR (1978) An electronic transition chemical laser. *Appl Phys Lett* 32(8):469–470, doi:10.1063/1.90088, <http://link.aip.org/link/?APL/32/469/1>

- Nikolaev V, Zagidullin M (2000) An efficient supersonic COIL with more than 200 Torr of total pressure in the active medium. In: Proceedings of the 31st AIAA plasmadynamics and lasers conference, AIAA Paper 2000-2427
- Nikolaev V, Zagidullin M, Svistun M, Anderson B, Tate R, Hager G (2002) Results of small-signal gain measurements in a supersonic chemical oxygen iodine laser with an advanced nozzle bank. *IEEE J Quantum Electron* 38(5):421–428
- Noren C, Vorobieff P, Truman C, Madden T (2010) Mixing in a supersonic COIL laser: influence of trip jets. *Exp Fluids* 50(2):443–455
- Pannu S, Johannesen N (1976) The structure of jets from notched nozzles. *J Fluid Mech* 74(3):515–528
- Prasad R, Sreenivasan K (1990) The measurement and interpretation of fractal dimensions of the scalar interface in turbulent flows. *Phys Fluids A* 2:792–807
- Ragheb A, Elliott G, King D, Laystrom-Woodard J, Carroll D, Solomon W (2010a) Low pressure schlieren imaging of a multi-stream injection nozzle. In: Proceedings of the 41st plasmadynamics and lasers conference, June 28–July 1, 2010, Chicago, Illinois, AIAA Paper 2010-4756
- Ragheb A, Elliott G, Laystrom J, King D, Carroll D, Solomon W (2010b) Low pressure PLIF visualization and mixing quantification in a multi-stream injection nozzle. In: Proceedings of the 48th AIAA aerospace sciences meeting, Orlando, FL, 4–7 January, 2010, AIAA Paper 2010-1439
- Rightley PM, Vorobieff P, Martin R, Benjamin RF (1999) Experimental observations of the mixing transition in a shock-accelerated gas curtain. *Phys Fluids* 11(1):186–200, doi:10.1063/1.869911, <http://link.aip.org/link/?PHF/11/186/1>
- Rybalkin V, Katz A, Barmashenko B, Rosenwaks S (2003) A 33% efficient chemical oxygen–iodine laser with supersonic mixing of iodine and oxygen. *Appl Phys Lett* 82:3838, doi:10.1063/1.1580634
- Sakurai K, Capelle G, Broida H (1971) Measurements of lifetimes and quenching cross sections of the $B_3\Pi_{O_u}$ state of iodine using a tunable dye laser. *J Chem Phys* 54(3):1220–1223
- Theiler J (1990) Estimating fractal dimension. *J Opt Soc Am* 7(6):1055–1073
- Truesdell K, Lamberson S, Hager G (1992) Phillips Laboratory COIL technology overview. In: Proceedings of the 23rd AIAA plasmadynamics and lasers conference, AIAA Paper 92-3003
- Truesdell RA, Vorobieff PV, Sklar LA, Mammoli AA (2003) Mixing of a continuous flow of two fluids due to unsteady flow. *Phys Rev E* 67(6):066304. doi:10.1103/PhysRevE.67.066304
- Vorobieff P, Rightley PM, Benjamin RF (1999) Shock-driven gas curtain: fractal dimension evolution in transition to turbulence. *Phys D Nonlinear Phenom* 133(1–4):469–476. doi:10.1016/S0167-2789(99)00079-2, <http://www.sciencedirect.com/science/article/B6TVK-3XG1SXXG-13/2/Ob5ec6052320f28cc68db41575e390a4>